Original Article

Quantitative assessment of intratumoral 2-[^{18}F]FDG metabolic spatial distribution in hypermetabolic pulmonary lesions in PET/CT

Ling Wang[1,2], Jia Jiang[3], Beihui Xue[3], Jie Lin[1], Xiaowei Ji[1], Xiangwu Zheng[3], Kun Tang[1]

[1]Department of Nuclear Medicine, The First Affiliated Hospital of Wenzhou Medical University, Wenzhou, China; [2]Key Laboratory of Clinical Laboratory Diagnosis and Translational Research of Zhejiang Province, The First Affiliated Hospital of Wenzhou Medical University, Wenzhou, China; [3]Department of Radiology, The First Affiliated Hospital of Wenzhou Medical University, Wenzhou, China

Correspondence to: Kun Tang, MD, PhD. Department of Nuclear Medicine, The First Affiliated Hospital of Wenzhou Medical University, Xuefu North Road, Wenzhou 325000, China. Email: kuntang007@163.com.

Background: The purpose of this study was to evaluate the value of quantitative assessment of intratumoral 2-deoxy-2-[^{18}F]fluoro-D-glucose (2-[^{18}F]FDG) metabolic spatial distribution (Q-FMSD) in differentiating pulmonary lesions with high 2-[^{18}F]FDG uptake.

Methods: In this retrospective study, a total of 564 patients with pulmonary lesions who underwent 2-[^{18}F]FDG positron emission tomography/computed tomography (PET/CT) examination were analyzed. The maximum standard uptake value (SUVmax) of the proximal (pSUVmax) and distal (dSUVmax) regions of the lesions were measured, respectively. Then, Q-FMSD was obtained by the ratio of pSUVmax to dSUVmax. The diagnostic performance and area under receiver operating characteristic curve (AUC) were compared between Q-FMSD and conventional PET/CT methods for the diagnosis of pulmonary lesions with high 2-[^{18}F]FDG uptake.

Results: The malignant tumors presented significantly higher Q-FMSD values than the benign lesions (1.11 *vs.* 0.94, P<0.001), which indicated that the 2-[^{18}F]FDG uptake in the proximal region was significantly higher than that of distal region in malignant lesions when compared with benign ones. For distinguishing hypermetabolic pulmonary malignant and benign lesions, the sensitivity, specificity and accuracy of Q-FMSD were 96.9%, 83.2% and 92.7%, respectively. Compared with other traditional methods, Q-FMSD presented significantly higher specificity than visual PET/CT (61.8%, P<0.001), retention index (RI) (33.8%, P<0.001) and SUVmax (11.0%, P<0.001). The AUC of Q-FMSD was 0.920, which was obviously larger than that of the SUVmax (0.587, P<0.001), RI (0.701, P<0.001), and visual PET/CT (0.781, P<0.001).

Conclusions: Q-FMSD provides a simply and quantitative indicator for differentiating hypermetabolic pulmonary lesions with higher diagnostic performance than conventional PET/CT methods. Therefore, Q-FMSD should be recommended as a new promising marker to improve the diagnostic performance of hypermetabolic pulmonary lesions in clinical practice.

Keywords: Fluorodeoxyglucose (^{18}F); positron emission tomography (PET/CT); metabolic; distribution; lung nodules; maximum standard uptake value (SUVmax)

Submitted Nov 26, 2021. Accepted for publication Apr 13, 2022.
doi: 10.21037/qims-21-1148
View this article at: https://dx.doi.org/10.21037/qims-21-1148

Introduction

Lung cancer is the leading cause of cancer-related deaths in the United States (1). Early detection and surgical resection are the best options for reducing lung cancer mortality (2). Positron emission tomography/computed tomography (PET/CT) has been widely used in differential diagnosis of pulmonary lesions (3-5). The maximum standard uptake value (SUVmax) is a common semiquantitative parameter for PET to evaluate the 2-deoxy-2-[18F]fluoro-D-glucose (2-[18F]FDG) uptake in tumors. However, 2-[18F]FDG is not a tumor specific agent, the overlaps of SUVmax between benign and malignant pulmonary lesions were observed in a large percentage of patients (6,7). Then, the accuracy of SUVmax in differential diagnosis of pulmonary lesions is limited. Therefore, a novel alternative diagnostic parameter based on PET is urgently needed to improve the diagnostic value for pulmonary lesions.

Heterogeneity is one of the significant characteristics of malignant tumors. Previous literature has demonstrated the heterogeneity of glucose metabolism in lung tumors (8). As an analogue of glucose, 2-[18F]FDG reflects the level of cellular glucose metabolism. 2-[18F]FDG distribution in malignant diseases might be heterogeneous based on necrosis, angiogenesis, cell proliferation, blood flow and hypoxia. Thus, to characterize the intratumoral 2-[18F]FDG metabolic spatial distribution (FMSD) might be helpful for the differential diagnosis between benign and malignant pulmonary lesions. Due to the different main blood supply, the blood perfusion and metabolic distribution between pulmonary benign and malignant lesions may be different. During tumor development and progression, cancer cells migrate to and invade blood vessels (9). Therefore, it can be assumed that cell metabolic activity in proximal region will be higher than that of distal region in malignant pulmonary lesions. Our published findings had firstly confirmed that the relative activity distribution (RAD) of 2-[18F]FDG in benign and malignant nodules was significantly different (10). Moreover, the specificity of 2-[18F]FDG RAD was much higher than that of conventional PET methods in differential diagnoses of solitary pulmonary nodules (SPNs). However, the acquisition of RAD requires complex diameter measurement and calculation, which limits its clinical application. Recently, we visually assessed the 2-[18F]FDG spatial distribution in pulmonary lesions (11). Although this simple procedure could improve the diagnostic performance for hypermetabolic pulmonary nodules and masses, the main limitation lied in the subjective bias of observers, and the interobserver agreement needed to be further improved.

In this study, we attempt to further explore a novel and simple quantitative method to objectively investigate the value of 2-[18F]FDG metabolic spatial distribution in differentiating pulmonary lesions with high 2-[18F]FDG uptake. We present the following article in accordance with the STARD reporting checklist (available at https://qims.amegroups.com/article/view/10.21037/qims-21-1148/rc).

Methods

Patients

From September 2016 to January 2019, a total of 564 consecutive patients (359 men and 205 women; mean age 62.3±10.9 years; range, 23–88 years) who underwent 2-[18F]FDG PET/CT for suspect malignant pulmonary lesions were included in this retrospective study. Inclusion criteria of the subjects were listed as follows: (I) all malignant lesions were confirmed as primary pulmonary tumors by pathology, and the diagnoses of all benign lesions were based on either pathology or at least 2 years of clinical follow-up; (II) diameter of lesions ≥10 mm; (III) pulmonary lesions with SUVmax higher than the mediastinal blood pool. The exclusion criteria were the subjects who: (I) had multiple hypermetabolic nodules or masses in both lungs; (II) had evidence of distant metastasis; (III) received previous lung biopsy or preoperative treatment; (IV) had previous history of other cancer; (V) had obvious breathing or motion artifact. The flow diagram was depicted in *Figure 1*. The study was conducted in accordance with the Declaration of Helsinki (as revised in 2013). The Institutional Ethics Committee of the First Affiliated Hospital of Wenzhou Medical University approved this retrospective study, and written informed consent was obtained from all included patients.

PET/CT acquisition

After at least 6 hours of fasting, the patients received an intravenous injection of 2-[18F]FDG (3.7 MBq/kg). Approximately one hour later, the PET/CT (GEMINI TF 64, Philips, Netherlands) scan was performed. For attenuation correction, low-dose unenhanced CT was performed with the following parameters: tube voltage 120 kVp, tube current 249 mA, detector collimation 64 mm × 0.625 mm, pitch 0.829, tube rotation speed 0.5 s, section thickness 5 mm, reconstruction thickness 2.5 mm. After CT scanning,

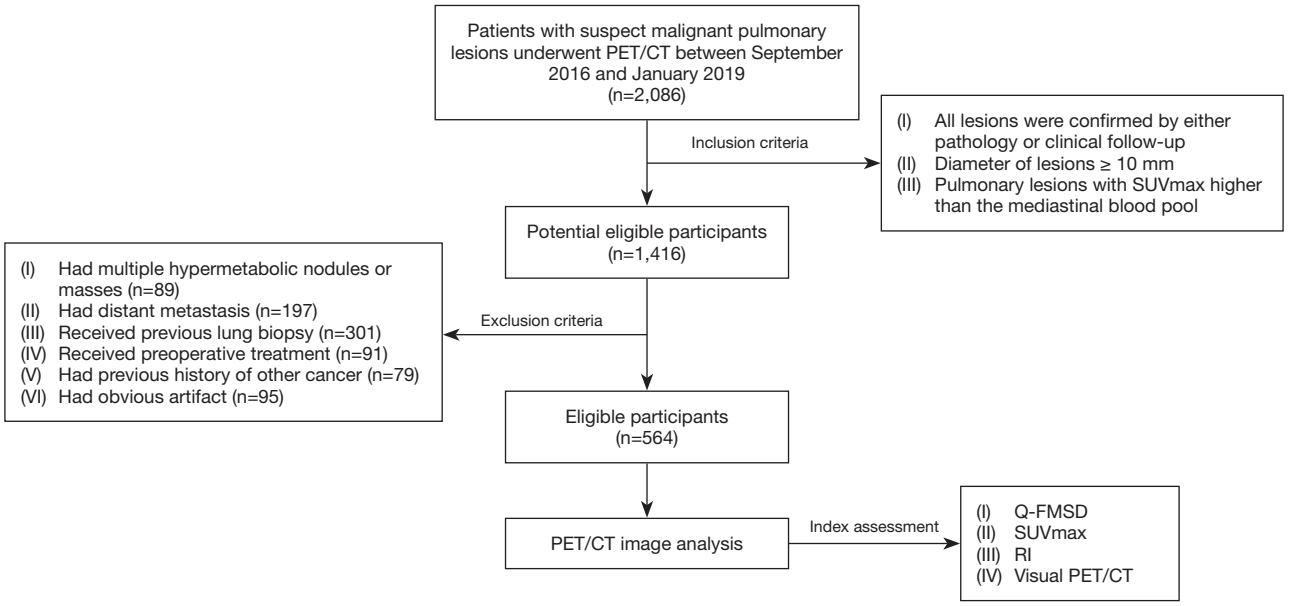

Figure 1 The flow diagram shows the process of patient enrollment. PET/CT, positron emission tomography/computed tomography; SUVmax, maximum standard uptake value; Q-FMSD, quantitative assessment of intratumoral 2-[^{18}F]FDG metabolic spatial distribution; RI, retention index.

a three-dimensional mode PET scan was obtained with the following parameters: field of view 576 mm, matrix 144×144, slice thickness 5 mm. PET images were iteratively reconstructed using the ordered subset expectation maximization (OSEM) algorithm. Finally, all collected data are transferred to Philips extended intelligence workstation 3.0 (EBW 3.0, Philips) to reconstruct PET, CT and PET/CT fusion images.

Image analysis

The 2-[^{18}F]FDG PET/CT data measurements and image analyses were performed on the Philips dedicated workstation. The SUVmax values of early and delayed scans were independently measured by one experienced nuclear medicine physician using the automatic method for delineation of the volume of interest (VOI). The SUVmax was defined as the highest value within the VOI. The retention index (RI) was calculated using the following formula: 100% × (delayed SUVmax-early SUVmax)/early SUVmax (10). For SUVmax assessment, the SUVmax ≥2.5 was considered as positive (12,13), and for RI assessment, RI >0 was defined as positive.

The visual PET/CT assessment was independently performed by two experienced nuclear medicine physicians who were ignored the characteristics of FMSD and blinded to the pathological results. Any inconsistency between the two readers was resolved by consensus. The lesions were interpreted as malignant when the 2-[^{18}F]FDG uptake of which were significantly higher than the mediastinal blood pool. For the remaining lesions with mild 2-[^{18}F]FDG accumulation, they were interpreted as probably malignant or probably benign based on the comprehensive judgments of CT morphological characteristics and PET metabolic information of lesions. Finally, malignant or probably malignant lesions were interpreted as positive and probably benign lesions were interpreted as negative.

The quantitative assessment of intratumoral 2-[^{18}F]FDG metabolic spatial distribution (Q-FMSD) was independently analyzed by two other experienced nuclear medicine physicians who were blinded to the information of pathology. In case of inconsistency between the two readers, consensus was reached on a final measurement for the statistical analyses. The specific procedures performed on MIP images were as follows: Firstly, the lesion was divided into two regions taking the pulmonary hilar as a reference point. The region close to the ipsilateral hilar was defined as the proximal region, and the region away from the ipsilateral hilar was defined as the distal region. Secondly, VOIs of the lesion proximal and distal regions

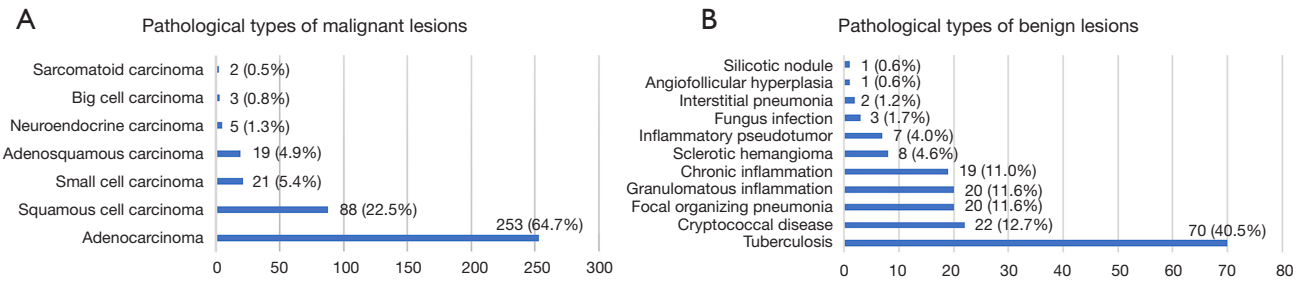

Figure 2 The pathological types of malignant and benign lesions.

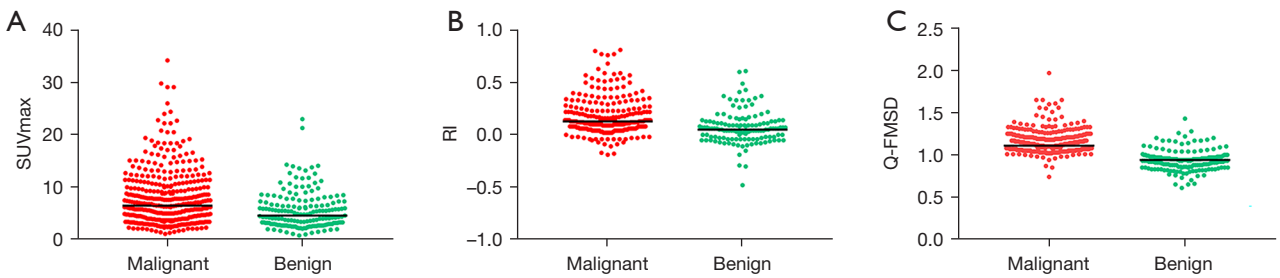

Figure 3 Scatter plots of SUVmax, RI and Q-FMSD. The horizontal line represents median value of each group. SUVmax, maximum standard uptake value; RI, retention index; Q-FMSD, quantitative assessment of intratumoral 2-[18F]FDG metabolic spatial distribution.

were drawn manually (14). Finally, SUVmax values of the proximal (pSUVmax) and distal (dSUVmax) regions were automatically obtained and the ratio of pSUVmax to dSUVmax (Q-FMSD) was subsequently calculated. The result was recorded as positive when Q-FMSD >1, and the result was recorded as negative when Q-FMSD ≤1 (10).

Statistical analysis

Since the distributions between benign and malignant groups were skewed, continuous variables were expressed as median and interquartile range (IQR), and the differences between groups were compared by independent sample Mann-Whitney test. For categorical data, presented as frequency and percentage, were analyzed by chi-squared test. Bland–Altman analysis was used to compare intra-observer variability in Q-MFSH. The diagnostic value of SUVmax, RI, visual PET/CT assessment and Q-FMSD for detection of malignance were calculated in terms of sensitivity, specificity, accuracy, positive predictive value (PPV) and negative predictive value (NPV). In addition, receivers operating characteristic (ROC) was plotted and the area under curve (AUC) was calculated to compare the capability of each method for distinguishing malignant and benign lesions. The McNemar test was analysed to compare the sensitivity, specificity and accuracy of Q-FMSD with other methods. All data were statistically analyzed using SPSS software, version 23.0 (IBM Corp., Armonk, New York, USA) and $P<0.05$ was considered to indicate statistical significance.

Results

General characteristics of subjects

Among all 564 lesions, the malignancy was proven in 391 (69.3%) lesions, and 173 (30.7%) lesions were benign. The median size of the lesion was 25.0 mm (range, 10 –159 mm). Among all patients, 383 (67.9%) cases were performed with delayed PET scans. The pathological types of malignant and benign lesions were shown in *Figure 2A,2B*. Among 564 lesions, significant differences were observed in lesion size, SUVmax, delay SUVmax and RI, whereby malignant tumors presented larger size, with significantly higher metabolic activity and RI than benign lesions (*Figure 3A,3B*). The comparisons of general characteristics between malignant and benign lesions were shown in *Table 1*.

Table 1 General characteristics of subjects

Characteristics	Overall (n=564)	Malignant (n=391)	Benign (n=173)	P value
Age, years, median (IQR)	63.0 (56.0, 69.0)	66.0 (58.0, 71.0)	59 (50.5, 66.0)	<0.001*
Sex, n (%)				0.039*
Male	359 (63.7)	238 (60.9)	121 (69.9)	
Female	205 (36.3)	153 (39.1)	52 (30.1)	
Smoking, n (%)	190 (33.7)	146 (37.3)	44 (25.4)	0.006*
Alcohol, n (%)	203 (36.0)	136 (34.8)	67 (38.7)	0.368
Diabetes, n (%)	92 (16.3)	70 (17.9)	22 (12.7)	0.124
Heart disease, n (%)	178 (31.6)	128 (32.7)	50 (28.9)	0.451
Tumor site, n (%)				0.341
RUL	168 (29.8)	113 (28.9)	55 (31.8)	
RML	38 (6.7)	29 (7.4)	9 (5.2)	
RLL	124 (22.0)	85 (21.7)	39 (22.5)	
LUL	141 (25.0)	105 (26.9)	36 (20.8)	
LLL	93 (16.5)	59 (15.1)	34 (19.7)	
Tumor size, mm, median (IQR)	25.0 (18.0, 35.0)	26.0 (20.0, 36.0)	20.0 (13.5, 33.5)	<0.001*
FBG (IQR), mmol/L, median (IQR)	5.4 (5.0, 6.2)	5.5 (5.0, 6.2)	5.3 (4.9, 6.2)	0.758
SUVmax, median (IQR)	5.8 (3.4, 9.2)	6.5 (3.8, 10.2)	4.6 (3.0, 7.2)	<0.001*
Delayed SUVmax, median (IQR)	6.0 (4.1, 9.7)	6.5 (4.2, 10.4)	4.8 (3.4, 7.6)	<0.001*
RI, %, median (IQR)	10.0 (4.0, 21.0)	13.0 (6.0, 24.0)	5.0 (3.0, 13.0)	<0.001*

*, significant difference (P<0.05) between malignant and benign groups. RUL, right upper lobe; RML, right middle lobe; RLL, right lower lobe; LUL, left upper lobe; LLL, left lower lobe; FBG, fasting blood glucose; SUVmax, maximum standard uptake value; RI, retention index; IQR, interquartile range.

The results of quantitative assessment of FMSD

Bland-Altman analysis showed excellent consistency between the two observers in measurement of Q-MFSH (P=0.455). The graph of Bland-Altman analysis was shown in Figure S1. Among all lesions, the median (IQR) value of Q-FMSD was 1.10 (0.98, 1.16). Compared with benign lesions, Q-FMSD of malignant tumors was significantly higher (P<0.001) (*Figure 3C*). The median (IQR) value of Q-FMSD in malignant tumors was 1.11 (1.06, 1.20), which indicated that the 2-[^{18}F]FDG metabolism distribution in the proximal region was significantly higher than that in the distal region (*Figure 4*). The median (IQR) value of Q-FMSD of benign lesions was 0.94 (0.86, 0.98), which indicated that the 2-[^{18}F]FDG metabolism distribution in the proximal region was significantly lower than that in the distal region (*Figure 5*). The comparison of Q-FMSD values between malignant and benign lesions among different size groups were shown in *Table 2*.

Diagnostic performance of different methods

The diagnostic performance of Q-FMSD in distinguishing benign and malignant lesions was shown in *Table 3*. When Q-FMSD >1 was considered as positive, the sensitivity, specificity, accuracy, PPV and NPV were 96.9%, 83.2%, 92.7%, 92.9%, and 92.3%, respectively. There was no significant difference in the sensitivity, specificity and accuracy of Q-FMSD method in the diagnosis of lesions of different sizes (P all >0.05). Compared with the conventional PET/CT method, although the sensitivity of Q-FMSD was similar to the other three methods (P all >0.05), the specificity and accuracy of Q-FMSD was

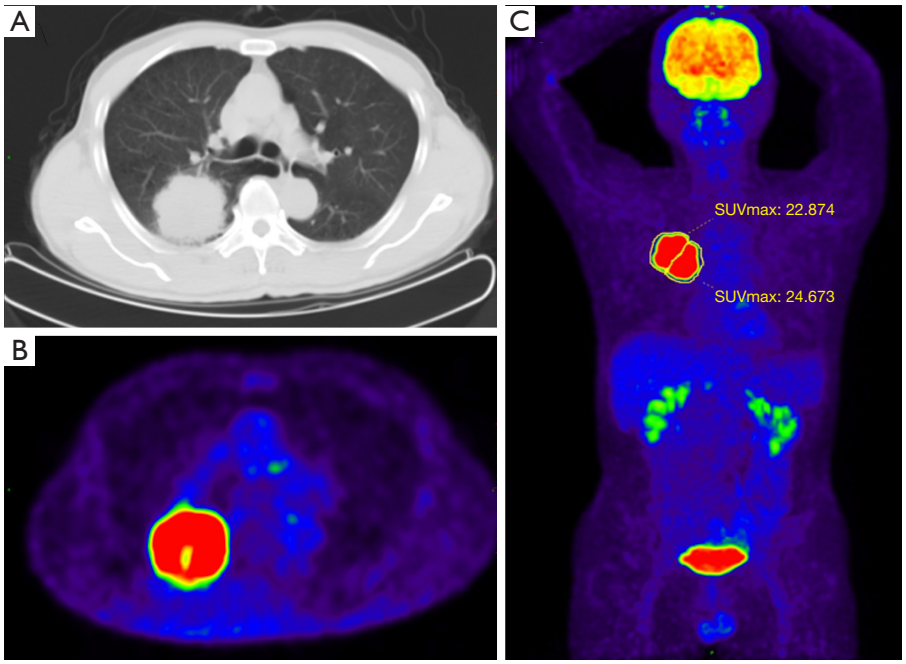

Figure 4 Images from a 69-year-old male patient with adenocarcinoma. Transaxial CT (A) showed a soft mass in the right upper lobe. The mass presented profound 2-[^{18}F]FDG uptake on transaxial PET image (B). The SUVmax values of the pSUVmax and dSUVmax regions were 24.673 and 22.874, respectively (C). The ratio of pSUVmax to dSUVmax was calculated as 1.079, which indicated a malignant lesion. PET, positron emission tomography; SUVmax, maximum standard uptake value; pSUVmax, proximal SUVmax; dSUVmax, distal SUVmax.

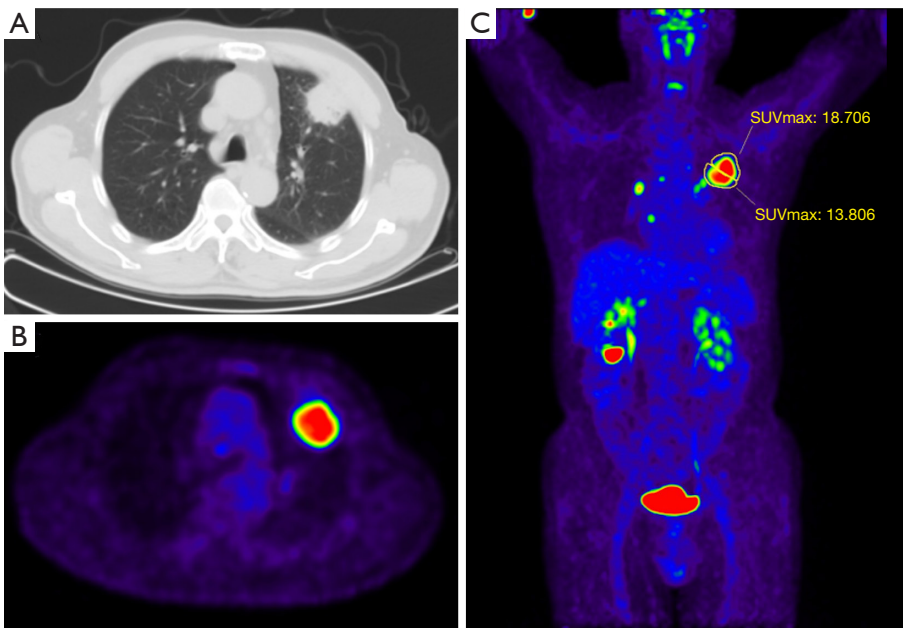

Figure 5 Images from a 73-year-old male patient with tuberculosis. Transaxial CT (A) showed a soft mass in the left upper lobe. The mass presented profound 2-[^{18}F]FDG uptake on transaxial PET image (B). The SUVmax values of the pSUVmax and dSUVmax regions were 13.806 and 18.706, respectively (C). The ratio of pSUVmax to dSUVmax was calculated as 0.738, which indicated a benign lesion. PET, positron emission tomography; SUVmax, maximum standard uptake value; pSUVmax, proximal SUVmax; dSUVmax, distal SUVmax.

Table 2 The Q-FMSD values of different size groups between malignant and benign lesions

Groups	Malignant	Benign	P
Overall, median (IQR), n=564	1.11 (1.06, 1.20)	0.94 (0.86, 0.98)	<0.001
10–19 mm, median (IQR), n=172	1.14 (1.09, 1.25)	0.94 (0.88, 0.97)	<0.001
20–29 mm, median (IQR), n=184	1.11 (1.05, 1.20)	0.94 (0.86, 0.98)	<0.001
30–49 mm, median (IQR), n=147	1.09 (1.04, 1.16)	0.92 (0.83, 0.99)	<0.001
≥50 mm, median (IQR), n=61	1.10 (1.04, 1.20)	0.95 (0.81, 0.99)	<0.001

Q-FMSD, quantitative assessment of intratumoral 2-[^{18}F]FDG metabolic spatial distribution; IQR, interquartile range.

Table 3 The performance of Q-FMSD for distinguishing benign and malignant lesions

Groups	TP	TN	FP	FN	Sensitivity	Specificity	Accuracy	PPV	NPV
Overall, n=564	379	144	29	12	96.9	83.2	92.7	92.9	92.3
10–19 mm, n=172	89	69	14	0	100.0	83.1	91.9	86.4	100.0
20–29 mm, n=184	140	36	6	2	98.6	85.7	95.7	95.9	94.7
30–49 mm, n=147	110	23	7	7	94.0	76.7	90.5	94.0	76.7
≥50 mm, n=61	40	16	2	3	93.0	88.9	91.8	95.2	84.2

Q-FMSD, quantitative assessment of intratumoral 2-[^{18}F]FDG metabolic spatial distribution; TP, true positive; TN, true negative; FP, false positive; FN, false negative; PPV, positive predictive value; NPV, negative predictive value.

Table 4 Comparison of diagnostic value among different methods

	TP	TN	FP	FN	Sensitivity	Specificity	Accuracy	PPV	NPV
Q-FMSD	379	144	29	12	96.9	83.2*	92.7*	92.9	92.3
Visual PET/CT assessment	380	107	66	11	97.2	61.8	86.3	85.2	90.7
Dual time point RI (%) >0	226	45	88	24	90.4	33.8	70.8	72.0	65.2
SUVmax ≥2.5	370	19	154	21	94.6	11.0	69.0	70.6	47.5

*, significant difference (P<0.001) between Q-FMSD and visual PET/CT, dual time point RI and SUVmax. TP, true positive; TN, true negative; FP, false positive; FN, false negative; PPV, positive predictive value; NPV, negative predictive value; Q-FMSD, quantitative assessment of intratumoral 2-[^{18}F]FDG metabolic spatial distribution; PET/CT, positron emission tomography/computed tomography; RI, retention index; SUVmax, maximum standard uptake value.

significantly higher than that of SUVmax (P<0.001), RI (P<0.001) and visual PET/CT (P<0.001) (*Table 4*). The confusion matrixes between Q-FMSD and SUVmax, RI, visual PET/CT were shown in *Figure 6*.

The ROC curves plotted by different indicators for comparison of diagnostic performance were demonstrated in *Figure 7*. The optimal cut off for the SUVmax was 6.15 from the ROC analysis. The corresponding diagnostic sensitivity and specificity were 34.4% and 79.7%, respectively. The AUC of SUVmax, RI, visual PET/CT assessment and Q-FMSD was 0.587, 0.701, 0.781 and 0.920, respectively. Compared with SUVmax, RI and visual PET/CT, the AUC of Q-FMSD was significantly larger (P all <0.001) (*Table 5*), which indicated the diagnostic performance of Q-FMSD was better than other three indicators.

Discussion

In the present study, we quantitatively evaluated the usefulness of intratumoural metabolic spatial distribution on 2-[^{18}F]FDG PET for distinguishing hypermetabolic pulmonary malignant and benign lesions. There was

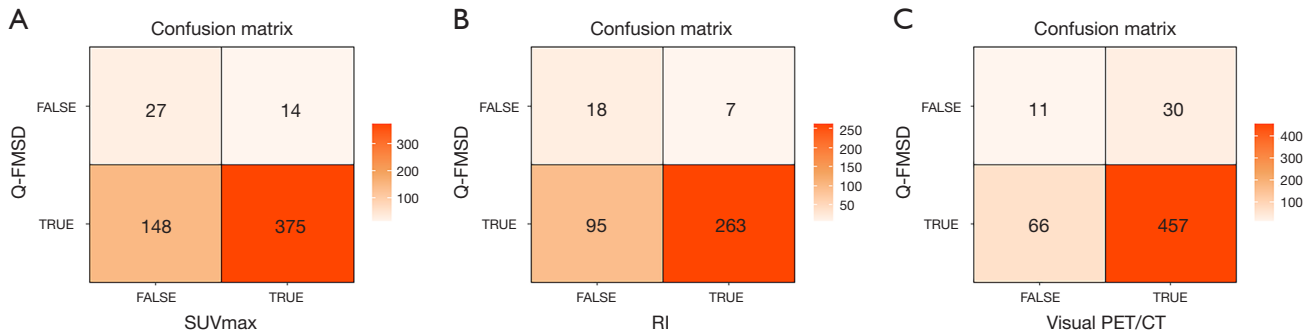

Figure 6 The confusion matrixes between Q-FMSD and SUVmax, RI, visual PET/CT. Q-FMSD, quantitative assessment of intratumoral 2-[18F]FDG metabolic spatial distribution; SUVmax, maximum standard uptake value; RI, retention index; PET/CT, positron emission tomography/computed tomography.

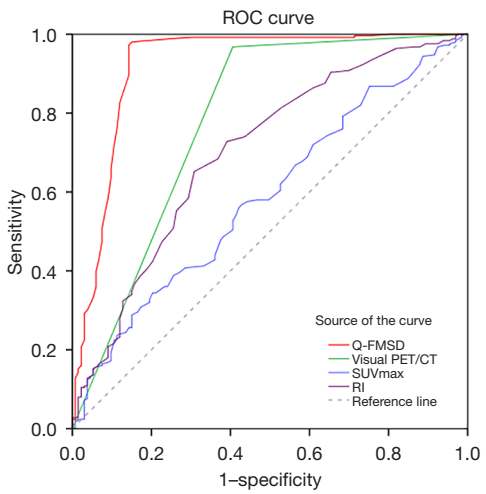

Figure 7 The ROC curves plotted by SUVmax, RI, visual PET/CT and Q-FMSD for comparison of diagnostic performance. ROC, receiver operating characteristic; SUVmax, maximum standard uptake value; RI, retention index; PET/CT, positron emission tomography/computed tomography; Q-FMSD, quantitative assessment of intratumoral 2-[18F]FDG metabolic spatial distribution.

significant distribution of tracer in proximal and distal region between pulmonary benign and malignant lesions. Furthermore, the characteristic of Q-FMSD could identify hypermetabolic pulmonary malignant tumors with higher diagnostic efficiency, especially for specificity, than other conventional PET/CT methods. Therefore, this study provides a simple and objective indicator to explore the benefits of intratumoural metabolic spatial distribution analysis in evaluating those pulmonary lesions with high 2-[18F]FDG uptake.

2-[18F]FDG PET/CT imaging, a noninvasive method, has been widely used in the clinical management of lung cancer (15,16). Alteration of tumor glucose metabolism is often determined by the concentration of 2-[18F]FDG, usually described as SUVmax (17). Generally, the malignant lesions have higher SUVmax than the benign ones, which are consistent with our findings. However, due to the high expression of glucose transporters in activated leucocytes, T-lymphocytes and macrophages (18-20), increased 2-[18F]FDG uptake can be found in a large proportion

Table 5 Comparison of AUCs among different methods

Variable(s)	Area	Std. Error	Significance	95% CI		Z value	P value
				Lower	Upper		
Q-FMSD	0.920	0.018	0.000	0.884	0.956		
Visual PET/CT assessment	0.781	0.028	0.000	0.726	0.836	4.212[a]	<0.001[a]
Dual time point RI	0.701	0.029	0.000	0.645	0.757	6.441[b]	<0.001[b]
SUVmax	0.587	0.030	0.000	0.528	0.646	9.514[c]	<0.001[c]

[a], Q-FMSD *vs*. visual PET/CT; [b], Q-FMSD *vs*. RI; [c], Q-FMSD *vs*. SUVmax. AUC, area under the ROC curves; Q-FMSD, quantitative assessment of intratumoral 2-[18F]FDG metabolic spatial distribution; PET/CT, positron emission tomography/computed tomography; RI, retention index; SUVmax, maximum standard uptake value.

of activated inflammation and granulomatous diseases, such as tuberculosis, cryptococcosis, sarcoidosis and so on (21-23). Then, the value of SUVmax in differentiating malignant and benign lesions is limited. Furthermore, the high incidence of tuberculosis in population may result in lower diagnostic efficacy of SUVmax in evaluation of hypermetabolic pulmonary lesions (24). In our study, tuberculosis accounted for 40.5% (70/173) of all benign lesions, and we found that the diagnostic specificity was only 11.0% when using SUVmax ≥2.5 as a positive indicator. For improving the diagnostic specificity of pulmonary lesions, dual time point scans were suggested. Still, the usefulness of this delayed scan is controversial (25). Although PET/CT combines CT morphology and PET metabolic information, the diagnostic specificity of PET/CT for detecting pulmonary nodules with high uptake 2-[^{18}F]FDG was variable, which was primarily associated with the possibility of high false positive results (24,26,27). Therefore, new alternative diagnostic indicators based on PET should be explored for enhancing the efficacy of imaging in diagnosis of hypermetabolic nodules.

Our previous study has shown that the metabolic distribution of 2-[^{18}F]FDG in malignant nodules was different from that of benign ones (10). Generally, the 2-[^{18}F]FDG uptake in the proximal region of malignant lesion was higher than that in the distal region, which was also proved by our visual assessment of the spatial distribution of 2-[^{18}F]FDG metabolism (11). Although the visual method can be used as an auxiliary indicator to improve the diagnostic accuracy of pulmonary lesions with high 2-[^{18}F]FDG uptake, the analysis was a subjective empirical judgment method which may lead to subjective bias.

Based on the spatial distribution of 2-[^{18}F]FDG uptake between proximal and distal region of malignant tumor, the present study firstly established a quantitative and easy-performed parameter of Q-FMSD for differential diagnosing of high metabolic lung lesions. Compared with previous visual analysis, Q-FMSD is a more objective index and less limited by the size of lesions. The median values of Q-FMSD in malignant and benign lesions were 1.11 and 0.94, respectively. Compared with benign lesions, Q-FMSD of malignant tumors was significantly higher. Moreover, our results revealed that the Q-FMSD values of malignant lesions in different size groups were all significantly higher than that of benign lesions. Those findings further confirmed the metabolic spatial distribution of lung cancer, namely, the 2-[^{18}F]FDG uptake in the proximal region of lung cancer was significantly higher than that of the distal region. For benign lesions, the 2-[^{18}F]FDG spatial distribution was opposite to that of the malignant lesions. The sensitivity, specificity and accuracy of Q-FMSD in distinguishing benign and malignant lesions were 96.9%, 83.2% and 92.7%, respectively. Compared with other traditional methods, the specificity and accuracy of Q-FMSD were obviously higher than visual PET/CT assessment, RI and SUVmax. Similarly, Q-FMSD presented higher diagnostic efficacy than the three conventional PET/CT indexes by using ROC curves analysis (AUCs: 0.886 *vs.* 0.781, 0.701, 0.587). It was indicated that Q-FMSD can be used as an objective and accurate indicator in diagnosis and differential diagnosis of pulmonary lesions. Recently, radiomics is a promising field related to the extraction of a set of features from CT or PET images to characterize malignant and benign lung lesions, even in those lesions without an altered glucose metabolism (28). We speculate that the radiomics characteristics based on different metabolic regions of lesions may provide important information for the identification of benign and malignant pulmonary lesions, which will be a subject worthy of in-depth research in the future.

However, the underlying pathological mechanism of the metabolic spatial distribution in benign and malignant pulmonary lesions was still uncertain. It has been proven that angiogenesis plays an important role in the occurrence and development of tumors (29-32). Tumor neovascularization may cause alteration in blood volume, perfusion and capillary permeability, which is different from activated inflammatory lesions. Then, angiogenesis and its distribution may be one of the possible reasons for the difference of metabolic distribution between benign and malignant lung lesions. Our pre-experiment findings had revealed that the expression of epidermal growth factor receptor (EGFR) and CD31 in the proximal region of pulmonary malignant lesion was higher than that in the distal region, suggesting that the difference of metabolic distribution may be correlated with tumor angiogenesis. Another possible reason may be related to the different blood supply between benign and malignant pulmonary lesions. The main blood supply of pulmonary malignant lesion is bronchial artery, most of which originated from descending aorta. Different from lung cancer, inflammatory lesions are more likely to stimulate extrapulmonary circulation arteries to participate in blood supply. Therefore, this may be the main reason for different distribution of blood supply in the proximal and distal regions between lung cancer and inflammation. However,

influenced factors for metabolic distribution in pulmonary lesions are complicated, and many other factors, including tumor microenvironment, genetic heterogeneity and immune may be involved (8,33,34). Recent studies show that the uptake of 2-[18F]FDG in tumor is related to tumor associated macrophages (TAM) (35), and the spatial density and distribution of TAM in lung cancer are related to the occurrence and prognosis of lung cancer patients (36). Therefore, it can be speculated that the metabolic spatial distribution of lung cancer may be associated with the spatial distribution of TAMs in the tumor microenvironment.

This study has the following limitations. Firstly, there was a selection bias. Since patients with hypermetabolic nodules and masses were selectively included in this study, the higher proportion of tuberculosis might contribute to the main component of benign lesions. Meanwhile, the application of this novel indicator of Q-FMSD in hypometabolic lesions was not verified in this study. Secondly, in order to simplify the method, the values of SUVmax between proximal and distal regions of lesion was compared in this study. However, SUVmax is calculated based on the hottest uptake of the lesion, then it is not enough to reflect the metabolic information of the entire region of lesion. Thirdly, the molecular mechanisms referring metabolic spatial distribution did not fully investigated in this study. Therefore, prospective studies with possible related mechanisms should be explored in the future.

Conclusions

In conclusion, the characteristic of 2-[18F]FDG metabolic spatial distribution between pulmonary benign and malignant lesions was distinct different. As a quantitative parameter, Q-FMSD provides complementary information for differentiating hypermetabolic pulmonary lesions with higher diagnostic performance than conventional PET/CT methods. Therefore, the index may be beneficial for characterization of pulmonary lesions and is recommended to be used as a promising marker to improve the diagnostic performance of hypermetabolic pulmonary lesions in clinical practice.

Acknowledgments

We wish to thank Miss Janet Akoto Ampadu (Wenzhou Medical University) for her helpful reading of the manuscript.

Funding: This work was supported by Wenzhou Science and Technology Program (No. Y20210222) and Zhejiang Public Welfare Technology Application Research Project (No. LGF19H180012).

Footnote

Reporting Checklist: The authors have completed the STARD reporting checklist. Available at https://qims.amegroups.com/article/view/10.21037/qims-21-1148/rc

Conflicts of Interest: All authors have completed the ICMJE uniform disclosure form (available at https://qims.amegroups.com/article/view/10.21037/qims-21-1148/coif). The authors have no conflicts of interest to declare.

Ethical Statement: The authors are accountable for all aspects of the work in ensuring that questions related to the accuracy or integrity of any part of the work are appropriately investigated and resolved. The study was conducted in accordance with the Declaration of Helsinki (as revised in 2013). This study was approved by the Institutional Ethics Committee of the First Affiliated Hospital of Wenzhou Medical University. Written informed consent was obtained from all patients.

References

1. Siegel RL, Miller KD, Jemal A. Cancer statistics, 2019. CA Cancer J Clin 2019;69:7-34.
2. Patz EF Jr, Rossi S, Harpole DH Jr, Herndon JE, Goodman PC. Correlation of tumor size and survival in patients with stage IA non-small cell lung cancer. Chest 2000;117:1568-71.
3. Garcia-Velloso MJ, Bastarrika G, de-Torres JP, Lozano MD, Sanchez-Salcedo P, Sancho L, Nuñez-Cordoba JM, Campo A, Alcaide AB, Torre W, Richter JA, Zulueta JJ.

Assessment of indeterminate pulmonary nodules detected in lung cancer screening: Diagnostic accuracy of FDG PET/CT. Lung Cancer 2016;97:81-6.
4. Hu L, Pan Y, Zhou Z, Gao J. Application of positron emission tomography-computed tomography in the diagnosis of pulmonary ground-glass nodules. Exp Ther Med 2017;14:5109-13.
5. Tsushima Y, Tateishi U, Uno H, Takeuchi M, Terauchi T, Goya T, Kim EE. Diagnostic performance of PET/CT in differentiation of malignant and benign non-solid solitary pulmonary nodules. Ann Nucl Med 2008;22:571-7.
6. Feng M, Yang X, Ma Q, He Y. Retrospective analysis for the false positive diagnosis of PET-CT scan in lung cancer patients. Medicine (Baltimore) 2017;96:e7415.
7. Yu WY, Lu PX, Assadi M, Huang XL, Skrahin A, Rosenthal A, Gabrielian A, Tartakovsky M, Wáng YXJ. Updates on 18F-FDG-PET/CT as a clinical tool for tuberculosis evaluation and therapeutic monitoring. Quant Imaging Med Surg 2019;9:1132-46.
8. Hensley CT, Faubert B, Yuan Q, Lev-Cohain N, Jin E, Kim J, et al. Metabolic Heterogeneity in Human Lung Tumors. Cell 2016;164:681-94.
9. Khatau SB, Bloom RJ, Bajpai S, Razafsky D, Zang S, Giri A, Wu PH, Marchand J, Celedon A, Hale CM, Sun SX, Hodzic D, Wirtz D. The distinct roles of the nucleus and nucleus-cytoskeleton connections in three-dimensional cell migration. Sci Rep 2012;2:488.
10. Zhao L, Tong L, Lin J, Tang K, Zheng S, Li W, Cheng D, Yin W, Zheng X. Characterization of solitary pulmonary nodules with 18F-FDG PET/CT relative activity distribution analysis. Eur Radiol 2015;25:1837-44.
11. Lin J, Wang L, Ji X, Zheng X, Tang K. Characterization of 18F-fluorodeoxyglucose metabolic spatial distribution improves the differential diagnosis of indeterminate pulmonary nodules and masses with high fluorodeoxyglucose uptake. Quant Imaging Med Surg 2021;11:1543-53.
12. Maiga AW, Deppen SA, Mercaldo SF, Blume JD, Montgomery C, Vaszar LT, Williamson C, Isbell JM, Rickman OB, Pinkerman R, Lambright ES, Nesbitt JC, Grogan EL. Assessment of Fluorodeoxyglucose F18-Labeled Positron Emission Tomography for Diagnosis of High-Risk Lung Nodules. JAMA Surg 2018;153:329-34.
13. Lowe VJ, Fletcher JW, Gobar L, Lawson M, Kirchner P, Valk P, Karis J, Hubner K, Delbeke D, Heiberg EV, Patz EF, Coleman RE. Prospective investigation of positron emission tomography in lung nodules. J Clin Oncol 1998;16:1075-84.
14. Wu L, Cao G, Zhao L, Tang K, Lin J, Miao S, Lin T, Sun J, Zheng X. Spectral CT Analysis of Solitary Pulmonary Nodules for Differentiating Malignancy from Benignancy: The Value of Iodine Concentration Spatial Distribution Difference. Biomed Res Int 2018;2018:4830659.
15. Cremonesi M, Gilardi L, Ferrari ME, Piperno G, Travaini LL, Timmerman R, Botta F, Baroni G, Grana CM, Ronchi S, Ciardo D, Jereczek-Fossa BA, Garibaldi C, Orecchia R. Role of interim 18F-FDG-PET/CT for the early prediction of clinical outcomes of Non-Small Cell Lung Cancer (NSCLC) during radiotherapy or chemo-radiotherapy. A systematic review. Eur J Nucl Med Mol Imaging 2017;44:1915-27.
16. Madsen PH, Holdgaard PC, Christensen JB, Høilund-Carlsen PF. Clinical utility of F-18 FDG PET-CT in the initial evaluation of lung cancer. Eur J Nucl Med Mol Imaging 2016;43:2084-97.
17. Zhang F, Wu X, Zhu J, Huang Y, Song X, Jiang L. 18F-FDG PET/CT and circulating tumor cells in treatment-naive patients with non-small-cell lung cancer. Eur J Nucl Med Mol Imaging 2021;48:3250-9.
18. Huber H, Hodolic M, Stelzmüller I, Wunn R, Hatzl M, Fellner F, Lamprecht B, Rubello D, Colletti PM, Gabriel M. Malignant disease as an incidental finding at ^{18}F-FDG-PET/CT scanning in patients with granulomatous lung disease. Nucl Med Commun 2015;36:430-7.
19. Mochizuki T, Tsukamoto E, Kuge Y, Kanegae K, Zhao S, Hikosaka K, Hosokawa M, Kohanawa M, Tamaki N. FDG uptake and glucose transporter subtype expressions in experimental tumor and inflammation models. J Nucl Med 2001;42:1551-5.
20. Keijsers RG, van den Heuvel DA, Grutters JC. Imaging the inflammatory activity of sarcoidosis. Eur Respir J 2013;41:743-51.
21. Sánchez-Montalvá A, Barios M, Salvador F, Villar A, Tórtola T, Molina-Morant D, Lorenzo-Bosquet C, Espinosa-Pereiro J, Molina I. Usefulness of FDG PET/CT in the management of tuberculosis. PLoS One 2019;14:e0221516.
22. Chang JM, Lee HJ, Goo JM, Lee HY, Lee JJ, Chung JK, Im JG. False positive and false negative FDG-PET scans in various thoracic diseases. Korean J Radiol 2006;7:57-69.
23. Metser U, Even-Sapir E. Increased (18) F-fluorodeoxyglucose uptake in benign, nonphysiologic lesions found on whole-body positron emission tomography/computed tomography (PET/CT): accumulated data from four years of experience with PET/CT. Semin Nucl Med 2007;37:206-22.

24. Li Y, Su M, Li F, Kuang A, Tian R. The value of 18F-FDG-PET/CT in the differential diagnosis of solitary pulmonary nodules in areas with a high incidence of tuberculosis. Ann Nucl Med 2011;25:804-11.
25. Laffon E, de Clermont H, Begueret H, Vernejoux JM, Thumerel M, Marthan R, Ducassou D. Assessment of dual-time-point 18F-FDG-PET imaging for pulmonary lesions. Nucl Med Commun 2009;30:455-61.
26. Taralli S, Scolozzi V, Foti M, Ricciardi S, Forcione AR, Cardillo G, Calcagni ML. 18F-FDG PET/CT diagnostic performance in solitary and multiple pulmonary nodules detected in patients with previous cancer history: reports of 182 nodules. Eur J Nucl Med Mol Imaging 2019;46:429-36.
27. Niyonkuru A, Chen X, Bakari KH, Wimalarathne DN, Bouhari A, Arnous MMR, Lan X. Evaluation of the diagnostic efficacy of 18 F-Fluorine-2-Deoxy-D-Glucose PET/CT for lung cancer and pulmonary tuberculosis in a Tuberculosis-endemic Country. Cancer Med 2020;9:931-42.
28. Caruso D, Zerunian M, Daffina J, Polici M, Polidori T, Tipaldi MA, Ronconi E, Pucciarelli F, Lucertini E, Rossi M, Laghi A. Radiomics and functional imaging in lung cancer: the importance of radiological heterogeneity beyond FDG PET/CT and lung biopsy. Eur J Radiol 2021;142:109874.
29. Herbst RS, Onn A, Sandler A. Angiogenesis and lung cancer: prognostic and therapeutic implications. J Clin Oncol 2005;23:3243-56.
30. Folkman J. Angiogenesis in cancer, vascular, rheumatoid and other disease. Nat Med 1995;1:27-31.
31. Ma Q, Reiter RJ, Chen Y. Role of melatonin in controlling angiogenesis under physiological and pathological conditions. Angiogenesis 2020;23:91-104.
32. Kirsch M, Schackert G, Black PM. Angiogenesis, metastasis, and endogenous inhibition. J Neurooncol 2000;50:173-80.
33. Navin N, Kendall J, Troge J, Andrews P, Rodgers L, McIndoo J, Cook K, Stepansky A, Levy D, Esposito D, Muthuswamy L, Krasnitz A, McCombie WR, Hicks J, Wigler M. Tumour evolution inferred by single-cell sequencing. Nature 2011;472:90-4.
34. Wang L, Zhu B, Zhang M, Wang X. Roles of immune microenvironment heterogeneity in therapy-associated biomarkers in lung cancer. Semin Cell Dev Biol 2017;64:90-7.
35. Wang Y, Zhao N, Wu Z, Pan N, Shen X, Liu T, Wei F, You J, Xu W, Ren X. New insight on the correlation of metabolic status on 18F-FDG PET/CT with immune marker expression in patients with non-small cell lung cancer. Eur J Nucl Med Mol Imaging 2020;47:1127-36.
36. Zheng X, Weigert A, Reu S, Guenther S, Mansouri S, Bassaly B, Gattenlöhner S, Grimminger F, Pullamsetti S, Seeger W, Winter H, Savai R. Spatial Density and Distribution of Tumor-Associated Macrophages Predict Survival in Non-Small Cell Lung Carcinoma. Cancer Res 2020;80:4414-25.

Cite this article as: Wang L, Jiang J, Xue B, Lin J, Ji X, Zheng X, Tang K. Quantitative assessment of intratumoral 2-[^{18}F]FDG metabolic spatial distribution in hypermetabolic pulmonary lesions in PET/CT. Quant Imaging Med Surg 2022;12(7):3821-3832. doi: 10.21037/qims-21-1148

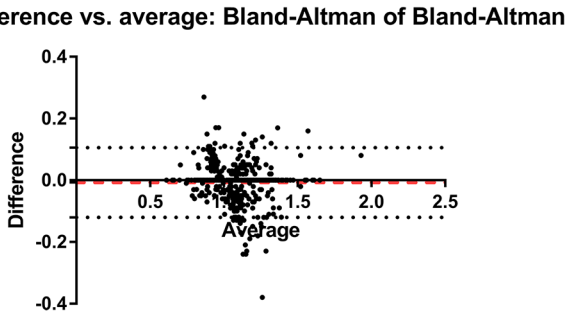

Figure S1 The graph of Bland-Altman analysis for comparison the variability between observers in Q-MFSD measurement. The mean value of the difference between the two observers was –0.0072, and the 95% confidence interval of the difference was –0.1201 to 0.1057. There was no statistical difference between the two observers (P=0.455), indicating good consistency in Q-MFSD measurement between observers. Q-FMSD, quantitative assessment of intratumoral 2-[^{18}F]FDG metabolic spatial distribution.

https://dx.doi.org/10.21037/qims-21-1148